HARVESTING ENERGY FROM MOTH VIBRATIONS DURING FLIGHT

S.C. Chang[1], F.M. Yaul[1], A. Dominguez-Garcia[3], F. O'Sullivan[2], D.M. Otten[1], J.H. Lang[1]
[1] EECS Department & [2] Energy Initiative, MIT, Cambridge, MA, 02139, USA
[3] ECE Department, University of Illinois, Urbana, IL, 61801

Abstract: This paper presents the design, fabrication, and testing of a harvester that extracts energy from moth-body vibrations during flight. The target moth is *manduca sexta*, which has a payload capacity near 1 g, and a dorsal payload volume approximately 8 mm wide and 15 mm tall. Operating within these constraints, the energy harvester is designed to deliver 1 mW of electrical power at 1 VDC for general-purpose use. It is based on magnetic induction driven by permanent magnets moving past windings. This motion is enhanced by a mechanical resonator tuned to the moth wing-flapping frequency.

Keywords: vibration energy harvesting; insect power; magnetic generator.

INTRODUCTION

This paper presents a harvester that extracts energy from moth-body vibrations during flight, and delivers it electrically for general-purpose use. Previous work on insect energy harvesting has compared concepts for moths [1], studied piezoelectric-based vibration harvesters for moths [2], and demonstrated 10 μW/cm^2 thermoelectric harvesting from beetles [3]. In contrast, this paper demonstrates the components of a magnetic-induction-based vibration energy harvester for the *manduca sexta* moth. The harvester is intended to deliver 1 mW at 1 VDC.

The payload capacity of *manduca sexta* is near 1 g. The mass of the harvester should be less to accomodate additional payloads, some to be powered by the harvester. The dorsal payload volume is tent shaped, with a 6-8 mm base, and a 10-15 mm height beneath the wings when they close at the apex of their flapping motion. The length of this volume can be 4-5 cm so long as the harvester mass distribution does not affect the aerodynamic balance of the moth.

Energy harvesting is implemented over two stages. The first stage is a reciprocating energy converter that is a linear AC poly-phase permanent-magnet synchronous generator. This generator is supported by a resonant spring-mass structure that enhances the moth wing-flapping vibrations; the generator magnets and cores serve as the resonating mass. The second stage comprises power electronics that rectify and condition the output from the generator for general-purpose use.

VIBRATION SOURCE

To determine the vibrations available for energy harvesting, high-speed filming is used to track the motion of a dorsal spot on *Manduca Sexta* between the wings during flight. A Fourier Transform of the recorded motion is shown in Figure 1, which identifies the 25-Hz components associated with wing flapping. The primary conclusion from the figure is that a narrow-band vibration of about $\pm$1 mm near 25 Hz, measured normal to the dorsal surface, is available for energy harvesting.

The narrow bandwidth of the wing-flapping moth vibrations argues for a resonant harvester employing a spring and proof mass to enhance the vibration stroke. A stroke of about $\pm$8 mm is allowed beneath the wings at the top of their motion. To achieve a 1-mW power output then requires the conversion of 40 μJ during each cycle with a peak force of 2.5 mN, assuming 100% energy-conversion efficiency from the generator and its attendant power electronics. This is incompatible with small low-mass low-voltage capacitive or piezoelectric energy conversion, and so a magnetic-based harvester is selected here.

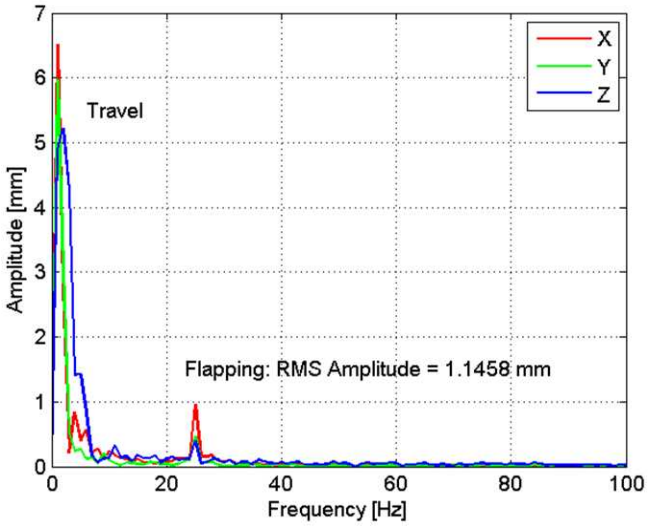

Figure 1: vibration Fourier Transform of *Manduca Sexta* during flight. The Z axis parallels gravity.

RESONANT GENERATOR

The resonant generator comprises a support structure, moving magnets and core, and stationary windings. The first three components form a spring-mass resonator tuned to the wing-flapping frequency of the moth; the structure is the spring, and the magnets and core provide the dominant proof mass. The magnets, core and windings form the linear poly-phase AC generator.

Figure 2 is one frame from a movie of a resonator attached to *manduca sexta*. The movie demonstrates that wing flapping is unaffected by the resonator, even when the resonator is elevated on a pedestal. The blurred motion of the moving mass is visible at the top of the photograph. Other experiments performed at the University of Washington demonstrate that *manduca sexta* can and will fly with a resonator attached.

Figure 3 shows the generator components assembled on a shaker table. The printed-circuit windings are stabilized from above, and supported by thin winding connections from below. An accelerometer, barely visible in the rear, is attached to the shaker frame. Connections to the power electronics are at the bottom of the photograph.

The spring is folded to be compact, and carry the magnets and cores level as they sweep vertically past the printed-circuit windings, as seen from the blurred motion in Figure 3. To limit horizontal motion, the spring is split into a left-half and right-half spring. Given the view of Figure 3, only one half spring can be seen; the second spring is behind the first. The structure/spring is printed in 3D from acrylonitrile butadiene styrene (ABS) plastic. The ABS is measured to have a 0.9-1.1 g/cm^3 mass density, a 2.1-GPa elasticity modulus, and a safe 0.6% yield strain. The ABS is printed layer-by-layer in orthogonal plys with a 0.07-in minimum feature size.

The magnets and magnetic cores, held by their ABS carrier, are shown in the top half of Figure 4. Three NdBFe magnets, each 9.5 mm wide, 1.8 mm tall, and 0.3 mm thick, are stacked vertically along 0.2-mm-thick cores attached to the carrier on each side of the air gap; there are six magnets in total. Spring segments from both sides can also be seen at the top and bottom of the photograph. The magnets are magnetized across their thickness to drive magnetic flux across the air gap. Their magnetization reverses from magnet to magnet along the cores in the direction of travel to form a three-pole magnetic structure.

The three-phase windings shown in the bottom half of Figure 4 are fabricated from two-sided 37-μm-thick printed-circuit copper on 13-μm-thick Kapton that is cropped in Figure 4. The Kapton extends much farther vertically, both up and down, as seen in Figure 3. Each phase winding contains two coils in a figure-eight pattern

Figure 2: energy harvester attached to *Manduca Sexta*. Courtesy of WM Tsang, MIT.

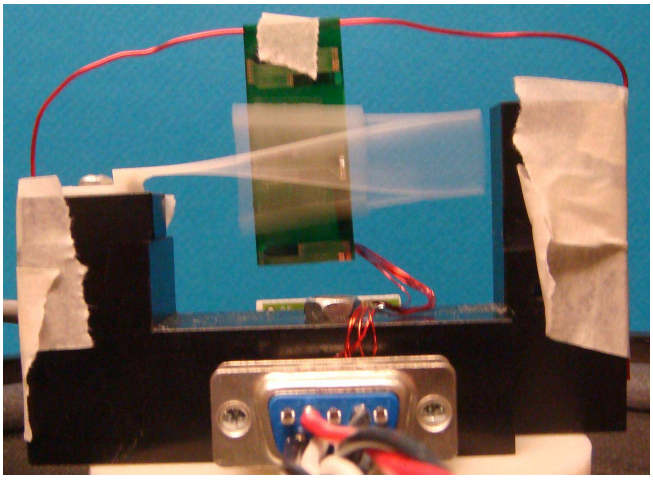

Figure 3: resonating generator on a shaker table.

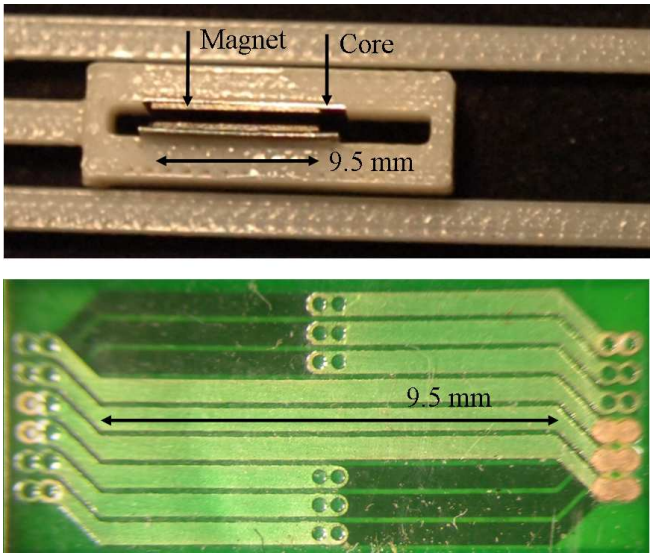

Figure 4: generator design and fabrication details.

that can link flux from two magnets. The windings match the 9.5-mm width of the magnets, and their vertical pitch matches the 1.8-mm magnet height; the long dimension of the magnets parallels to the long dimension of the winding coils. The winding terminations are located to permit easy stacking of a multi-layer winding. The generator in Figure 3 has two stacked layers.

The Kapton and windings slip inside the gap between the magnets in Figure 4, to make the generator shown in Figure 3. A 100-μm gap is left between the windings and the magnets on either side. The active windings are barely visible behind the blur in Figure 3, but unused windings are visible at the top of the Kapton sheet. As the resonator vibrates, the magnets sweep past the winding coils. This magnetic shearing maximizes the time-varying magnetic flux through the winding coils given the limited motion, in contrast to collinear-flux-motion designs [4].

The quality factor Q of the ABS resonator is near 60. With the windings inserted, the Q drops to near 40 indicating that the internal-ABS and sliding-friction losses are comparable. However, the losses are small compared to the electromechanical loading, which results in a Q of 10-25. During operation, the magnets typically swing well beyond the windings, but not beyond the Kapton. The extended Kapton guides the carrier.

The proof-mass mass combines six magnets at 240 mg, two cores at 180 mg, and the ABS carrier at 249 mg for a total of 669 mg. This mass yields a 25.8-Hz resonance frequency. The springs contribute 322 mg, and the Kapton and windings in Figure 3 contribute another 288 mg, for a 1.28-g total generator mass.

At 25 Hz, an appropriate model for each phase of the generator shown in Figure 3 is a speed voltage in series with a 118-mΩ winding resistance. To model the speed voltage, the peak flux linkages that occur as the various magnets align with the winding coils are found using magnetic circuit analysis [5]. A spline is then fit through the peaks to determine the flux linked by each phase as a function of displacement. The speed voltage is the time derivative of this flux linkage. Figure 5 shows balanced three-phase 0.110-Ω-loaded load-voltage waveforms when the shaker vibrates with a $\pm$0.37-mm amplitude at 25.8 Hz, resulting in a $\pm$7.82-mm generator amplitude, and a 1.7-mW output power to the load. The modeled generator terminal voltages are shown for comparison.

To explore the output power, the generator phases are loaded with balanced resistors. The shaker is set to vibrate with a $\pm$0.23-mm amplitude at 25.8 Hz. The resulting output power into the load resistors is shown in Figure 6 as a function of load resistance. The peak output power near 0.9 mW, which occurs with a generator amplitude

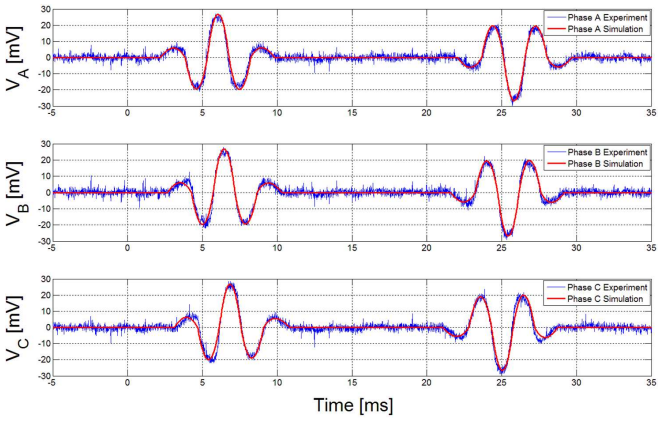

Figure 5: loaded generator voltage waveforms.

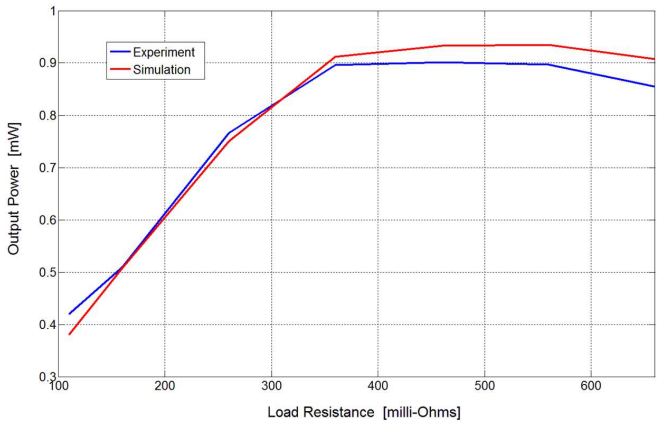

Figure 6: total generator output power.

of $\pm$7.0 mm, does not come with a matched load of 118 mΩ due to the electromechanical loading of the generator. In these experiments, the generator amplitude varies from $\pm$2.4 mm to $\pm$8.4 mm as the load resistance increases.

POWER ELECTRONICS

As shown in Figure 7, the power electronics operate to extract maximum power from the generator, and deliver that power to a 1-VDC load, through two stages. The first stage is a combined AC/DC rectifier and DC/DC boost converter. There is one such stage for each generator phase, and the outputs of these parallel stages deliver energy to a common intermediate energy storage capacitor at about 50 mV. Following the capacitor is a single DC/DC boost converter that raises the voltage from 50 mV to 1 V.

To deliver maximum power to the load, each first stage shuts down when input voltage magnitude falls below 10 mV. Each stage should also operate with a duty cycle that varies with phase voltage. This is not done here for simplicity, but at the expense of efficiency and output power. The duty cycle remains constant, but it is chosen

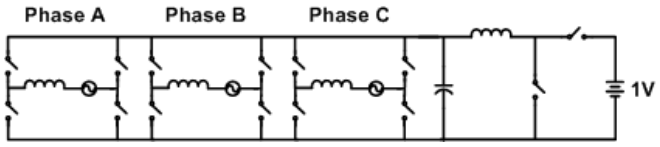

Figure 7: power electronics diagram.

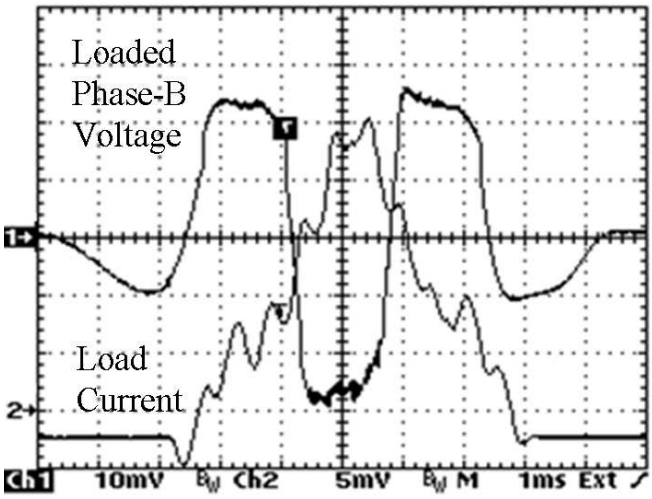

Figure 8: power electronics waveforms.

to maximize power throughput to the extent possible. The second-stage DC/DC converter should also shut down and operate with a variable duty cycle. Neither feature is implemented yet, again for simplicity at the expense of efficiency and output power.

The power electronics will ultimately be integrated, having an estimated 40-mg mass, exclusive of the inductors, and an 80% efficiency. However, in the experiments reported here the power electronics are implemented discretely, with power transistors, inductors, and an energy storage capacitor selected to best match the behavior of the integrated-circuit implementation. In particular, the inductor parameters are 10 μH, 0.01 Ω and 120 mg, and should contribute the dominant mass and loss within the integrated-circuit power electronics.

The discrete power electronics are combined with the harvester shown in Figure 3. The shaker vibrates with an amplitude of $\pm$0.81 mm at 25.8 Hz, resulting in a harvester amplitude of $\pm$7.0 mm. The resulting Phase-B voltage, and load current measured at 10 mV/mA, are shown in Figure 8. The load current is -0.2 mA when the second-stage boost converter is not operating. This is unintended, and considered here to be part of the load.

Power flow through the harvester can be estimated from the waveforms in Figure 8 and the generator model from Section 3. The converted three-phase generator power is estimated to be 0.84 mW, and the power into the load is measured to be 0.40 mW. The losses are estimated to be 0.16 mW in the generator phases, 0.1 mW in the generator-to-power-electronics wiring, and 0.18 mW in the power electronics. The generator and power electronics are 81% and 69% electrically efficient. The wiring losses can be eliminated by integrating the power electronics and the generator windings.

CONCLUSIONS

The objective of 1-mW energy harvesting from a 1-g payload has not yet been met, but the results described here are encouraging. The mass of the harvester can be reduced through judicious trimming. Harvester efficiency can be improved significantly by eliminating the wiring losses, by dynamically adjusting the converter PWM duty cycles, and by adjusting the times at which the converters turn on and off. Improving the power electronics operation with varying duty cycles and second-stage shut down should yield a load power of 0.95 mW during the 1.7-mW experiment of Figure 5. Integrated power electronics should perform better. Generator power might also be improved with additional winding layers, though there are eventually diminishing returns, and this adds extra mass.

ACKNOWLEDGEMENTS

The authors gratefully thank Professor Thomas Daniel and his group at the University of Washington, Seattle, for recording the vibrations that underly Figure 1. This work was supported by the Air Force Research Laboratory as part of the DARPA HI-MEMS Program under Contract FA8650-07-C-7704.

REFERENCES

[1] Reissman and Garcia, *Proceedings ASME SMASIS*, 711-718, Oct 2008.

[2] Reissman and Garcia, *Proceedings ASME IMECE*, 645-653, Nov 2008.

[3] Ghafouri, Kim, Atashbar and Najafi, *Proceedings IEEE Sensors Conference*, 1249-1252, May 2008.

[4] Amirtharajah and Chandrakasan, *IEEE JSSC*, 33, 687-695, May 1998.

[5] Fitzgerald, Kingsley and Umans, *Electric Machinery*, 6th edition, McGraw Hill, 2003.